Atmospheric Pollution Research 13 (2022) 101512

Contents lists available at ScienceDirect

Atmospheric Pollution Research

journal homepage: www.elsevier.com/locate/apr

Ambient concentrations and dosimetry of inhaled size-segregated particulate matter during periods of low urban mobility in Bragança, Portugal

Yago Alonso Cipoli [a,b], Admir Créso Targino [c], Patricia Krecl [c], Leonardo Campestrini Furst [a,b], Célia dos Anjos Alves [a], Manuel Feliciano [a,*]

[a] Centro de Investigação de Montanha (CIMO), Instituto Politécnico de Bragança, 5300-253, Bragança, Portugal
[b] Centre for Environmental and Marine Studies (CESAM), Department of Environment and Planning, University of Aveiro, 3810-193, Aveiro, Portugal
[c] Graduate Program in Environmental Engineering, Federal University of Technology, Londrina, PR, Brazil

ARTICLE INFO

Keywords:
Size-segregated particulate matter
Mobile monitoring
Lockdown
Exposure assessment
MPPD dosimetry Model

ABSTRACT

The restrictive measures in place during the COVID-19 pandemic provided a timely scenario to investigate the effects of human activities on air quality, and the extent to which mobility reduction strategies can impact atmospheric pollutant levels. Real-time concentrations of PM_1, $PM_{2.5}$ and PM_{10} were measured using a mobile platform in a small city of Portugal, during morning and afternoon rush hours, in two distinct phases of the pandemic: emergency phase (cold period, lockdown) and calamity phase (warm period, less restricted). The Multiple-Path Particle Dosimetry Model (MPPD) was used to calculate the PM deposition for adults. Large spatio-temporal variabilities and pronounced changes in mean PM concentrations were observed, with lower concentrations in the calamity phase: $PM_1 = 2.33 \pm 1.61$ μg m^{-3}; $PM_{2.5} = 5.15 \pm 2.77$ μg m^{-3}; $PM_{10} = 23.30 \pm 21.53$ μg m^{-3} than in the emergency phase: $PM_1 = 16.85 \pm 31.80$ μg m^{-3}; $PM_{2.5} = 30.92 \pm 31.93$ μg m^{-3}; $PM_{10} = 111.27 \pm 104.53$ μg m^{-3}. These changes are explained by a combination of meteorological factors and local emissions, mainly residential firewood burning. Regarding regional deposition, PM_1 was the main contributor to deposition in the tracheobronchial (5%) and pulmonary (12%) regions, and PM_{10} in the head region (92%). In general, total deposition doses were higher for males than for females. This work quantitatively demonstrated that even with a 38% reduction in urban mobility during the lockdown, the use of firewood for residential heating is the main contributor to the high concentrations of PM and the respective inhaled dose.

1. Introduction

The coronavirus disease 2019 (COVID-19), caused by the Sars-Cov-2 virus, spread rapidly around the world, affecting the health, economic, social and environmental domains, being declared in March 2020 as a global pandemic by the World Health Organisation (WHO, 2020). In Portugal, the first confirmed case was on the 2nd of March, and the first death was recorded on the 16th of that month. To fight the fast spread of the disease, contingency plans and restrictive measures - including school closures, mandatory confinements, closure of non-essential establishments, reduced mobility and transport - were put in place in the first week of March (DRE, 2021).

Global studies reported that this socioeconomic disruption had positive effects on the environment, especially on the regional air quality, with lower ambient concentrations for some air pollutants compared to the period before the pandemic (Collivignarelli et al., 2021; Krecl et al., 2020b; Sulaymon et al., 2021; Venter et al., 2020), except for tropospheric ozone which showed regional increases (Adam et al., 2021; Nie et al., 2021; Sicard et al., 2020). The decrease in ambient concentrations was more evident for exhaust pollutants arising from fossil-fuelled on-road vehicles (such as NOx) due to the mobility restrictions. However, this decreasing pattern was not as evident for particulate matter (PM) (Sokhi et al., 2021), which showed complex signals in relation to other pollutants. Some cities showed increases in PM concentrations due to secondary aerosol formation, biomass burning and long-range transport (Sun et al., 2020; Wang et al., 2021). The

Peer review under responsibility of Turkish National Committee for Air Pollution Research and Control.
* Corresponding author.
E-mail address: msabenca@ipb.pt (M. Feliciano).

https://doi.org/10.1016/j.apr.2022.101512
Received 2 May 2022; Received in revised form 18 July 2022; Accepted 19 July 2022
Available online 11 August 2022

northern regions of Spain and Portugal, particularly, experienced enhancements in PM concentrations (Menut et al., 2020; Querol et al., 2021) attributed to the increased use of biomass for residential heating, which greatly contributed to primary and secondary aerosols, since the citizens were instructed to stay home as much as possible during the lockdown.

The scientific literature has shown a well-established relationship between PM exposure and its association with increased morbidity, in terms of specific mass fractions (Chen et al., 2015; Liu et al., 2013; Samek et al., 2018) and species within the PM (Caggiano et al., 2019; Hassanvand et al., 2015).

The population circulating close to motorised traffic is usually exposed to high peaks of atmospheric pollutants, such as PM (particularly in terms of particle number and specific markers, such as black carbon) and NOx (Krecl et al., 2020a, 2019; Targino et al., 2016; Van den Bossche et al., 2016). Recently, it has been argued that the current 24-h standard for PM concentrations mask spikes occurring during the day, and that air quality mandates should consider shorter periods for threshold values, along with the assessment of the highest percentiles (e.g., 99th) (Nazarenko et al., 2021). The inhalation of airborne particles is one pathway for particles to enter the human body, which will be deposited later in different regions of the respiratory system. A large body of research about PM deposition in the pulmonary region focuses mainly on the total PM deposition, especially in adult males (Jia et al., 2020; Madureira et al., 2020; Prabhu et al., 2019). However, from an epidemiological and toxicological perspective, it is important to quantify the PM deposition and understand the response to pollution for different population groups, genders and in specific regions (extrathoracic: H, tracheobronchial: TB and pulmonary region: P) of the human respiratory tract (Kecorius et al., 2019; Lv et al., 2021).

Few studies have addressed PM deposition doses in pedestrians (Lv et al., 2021; Manigrasso et al., 2017; Menon and Nagendra, 2018), which commonly dominate the scene in multimodal chains. In this work, PM concentrations were monitored while cycling and used to assess the deposition in the respiratory system of pedestrians. Mobile monitoring with bicycles proved to be effective in covering an extensive area in a relatively short time compared to walking. Studies measuring on multiple transportation modals concluded that cyclists (de Nazelle et al., 2012; Kaur et al., 2005; McNabola et al., 2008) and pedestrians (Goel et al., 2015; Quiros et al., 2013) are more exposed than passive modals. Furthermore, cycling close to sidewalks showed substantial or irrelevant differences between the exposures found on the sidewalk (Pattinson et al., 2017).

In this study, we profit from a wealth of *in situ* real-time PM concentrations (PM_1, $PM_{2.5}$ and PM_{10}) collected on a mobile platform in the city of Bragança to analyse how they responded to the measures adopted in two contingency phases of the COVID-19 pandemic. For this reason, the objectives of the present work were to 1) evaluate the spatio-temporal variability of PM mass concentrations in different seasons, periods of the day and road configurations, 2) to investigate the impact of restriction measures during the COVID-19 pandemic on ambient concentrations of PM, and 3) to quantify the exposure and total and regional doses of different sizes of PM deposited in the human respiratory system for adults of both genders, through a pulmonary deposition modelling tool (MPPD), allowing stronger associations with health outcomes.

2. Methods

2.1. Study area

The study was conducted in Bragança (lat. 25° 440′N, long. 6° 480′W, alt. 690 m), a city with a population of 35,000 inhabitants in north-eastern Portugal (Pordata, 2021). The climate of the region is temperate with dry and hot summers (Csa in the Köppen-Geiger classification, Peel et al., 2007). Firewood is the main fuel for residential heating, totalling 17,000 tons per year, corresponding to an average of 4 tons per dwelling (Azevedo et al., 2016). As in other regions of the Iberian Peninsula, PM concentrations in Bragança increase sporadically as a result of long-range transport of forest fires smoke and intrusions of desert dust (Pereira et al., 2008; Fernández et al., 2019; Russo et al., 2020). In particular, the city does not have a fixed air quality station and has been the subject of very few PM monitoring studies (Dantas et al., 2019).

PM concentrations were monitored in the urban area (10 km^2) of the city along two prescribed routes (Fig. 1), covering an area of 3 km^2 with different road configurations, influences and traffic densities. The route selection was based on factors known for affecting the PM spatial distribution, such as the number of on-road vehicles, urban structures (e.g., tunnels and street canyons), proximity to sources of smoke from residential heating, and other PM emission sources (e.g., on-going construction activities). Traffic counts were manually measured at 14 points along the routes at times of the day coinciding with the mobile monitoring. The number of vehicles was counted by category (cars, motorcycles, buses, and trucks) in two 15-min intervals, alternating every 15 min with a break, following Targino et al. (2016). The hourly traffic volume at each counting point was estimated as twice the number of counts.

2.2. Monitoring and data collection protocols

2.2.1. Instrumentation

An optical particle sizer spectrometer (model OPS 3330, TSI, USA) was used to measure the ambient PM mass concentrations in 16 size channels (0.3 − 10 μm), with a threshold of 3000 #/cm^3 (total concentration). The OPS detection range was from 0.001 to 275,000 μg m^{-3}, with a size resolution of ±5% at 0.5 μm (TSI Inc., 2019). The OPS was operated with a flow rate of 1 L min^{-1} and a temporal resolution of 1 s, following the manufacturer's specifications. Before each sampling session, the following checks were performed: zero calibration, flow rate, battery, memory and clock synchronisation. PM concentrations

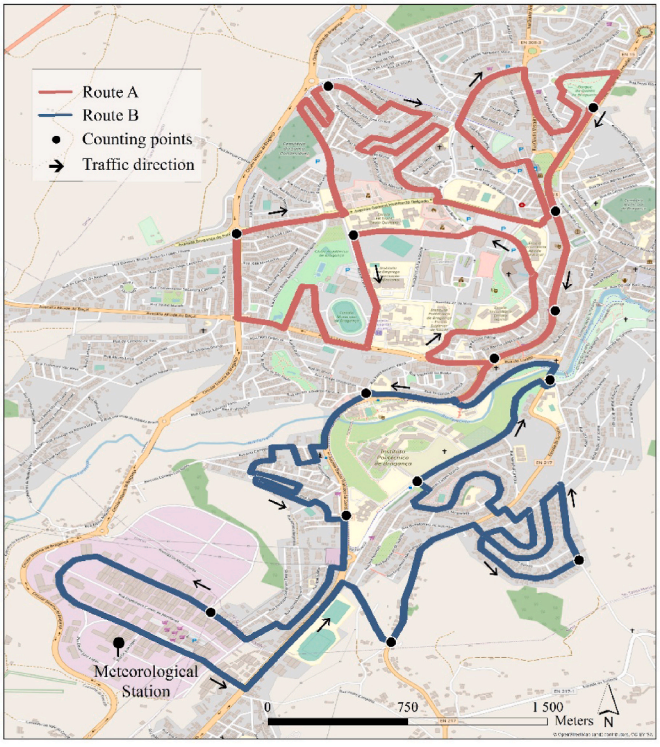

Fig. 1. - Map of the study area with the selected routes and traffic counting points.

provided by the OPS monitor were corrected against gravimetric measurements (see section 2.4). A GPS receiver and logger was operated simultaneously at a sampling frequency of 1 s to geo-reference the OPS measurements.

The OPS is a very practical, compact, and portable and has been used in a variety of applications to measure particle number concentrations and PM mass concentrations (Jing et al., 2014; Jasiński et al., 2021).

2.2.2. Monitoring campaigns

The mobile monitoring campaigns took place on 17 selected non-rainy days in the summer of 2020 and 14 non-rainy days in the winter of 2021 (Table S5, supplementary material), covering weekdays and weekends and during morning (9:00 to 11:00 local time) and afternoon rush hours (17:00 to 19:00 local time). Measurements were not performed on rainy days to avoid the removal of particles in the atmosphere, affecting ambient PM concentrations. The equipment was installed inside a bicycle basket (Fig. S1, Supplementary Material), about 70 cm from the ground, protected by plastic bubble wrap and foam materials to reduce vibration. The cyclist used a mobile phone to record audio that helped interpret outstanding PM concentration events along the route. The study comprised two routes of approximately 11 km each, with different urban configurations, number of vehicles, and land use. The data collection covered of 17 sampling sessions in the calamity phase and 14 sampling sessions in the emergency phase. All sampling sessions started at the same point and time, to minimise possible variations in the number of vehicles and to capture rush periods, and each session lasted between 1 and 2 h. A cycling speed of 10 km h^{-1} was adopted to measure PM concentrations with a fine spatial resolution (on average, one data point every 2.5 m). Cycling occurred as close as possible to the sidewalk (maximum of 1 m from pedestrians) to better represent the pedestrian's exposure (Pattinson et al., 2017).

2.2.3. Study period

The study was carried out from May 30 to June 21, 2020 (covering the state of calamity) and from February 15 to March 07, 2021 (covering the state of emergency). The fraction of population that stayed at home was used to assess the reduction in mobility during the pandemic (Fig. 2). The calamity phase was characterised by about 22% of the population staying at home, due to the recommended teleworking, reduction in opening hours of commercial establishments, and curfew applied at times. In January 2021, Portugal started the emergency phase and implemented stricter measures, resulting in 38% of the population spending more time at home. The measures imposed by the government lasted until March 15, after which there was a slow and gradual resumption. The emergency phase was characterised by the closure of schools, mandatory teleworking, mandatory confinement, travel with authorisations, and restricted curfews (DRE, 2021).

2.3. Data analysis

The PM_1, $PM_{2.5}$ and PM_{10} mass concentrations were obtained by integrating the following bins: 0.3–1 μm, 0.3–2.5 μm, and 0.3–10 μm, respectively. The PM concentrations and GPS location data were combined using a computer software that scanned for coincident timestamps and merged the occurrences, creating georeferenced points. Inaccurate or missing geolocation data (e.g., inside road tunnels) were fixed by reprojecting them onto the prescribed route using a GIS software, based on valid neighbouring data points of bike speed, distance travelled and the known cycling path. Descriptive statistics of size segregated PM were performed to identify differences between spatial, seasonal and temporal concentrations. Non-parametric tests (Mann-Whitney test at 5% significance level) were calculated to assess statistical differences between median pollutant concentrations. The spatial analysis followed the methodology by Targino et al. (2016) and Van den Bossche et al. (2016), in which streets along the two routes were segmented into 70-m polygons (310 polygons in total) and all data points that fell into each individual polygon were aggregated and used to calculate PM statistics for each segment. Each polygon contains on average 25 p.m. data points per sampling (Fig. S2, Supplementary Material).

2.4. Quality assurance and control

The OPS might have experienced deviations during sampling, depending on the response of optical equipment to different types of aerosols (Ramachandran and Cherian, 2008), and the calibration process is essential to ensure more accurate measurements. As we didn't have a any reference instrument was available for calibration during sampling period, we correlated data from two previous campaigns to correct OPS data. The calibration took place in two inter-comparisons steps: 1) OPS versus light-scattering laser photometer (DustTrak, Model 8533, TSI Inc., USA), and 2) DustTrak versus Echo sampling head (TECORA, model 2004.01, Italy). The TECORA sampler is certified by the European Committee for Standardization as a reference instrument for PM_{10} and $PM_{2.5}$ measurements according to EN 14907. Both

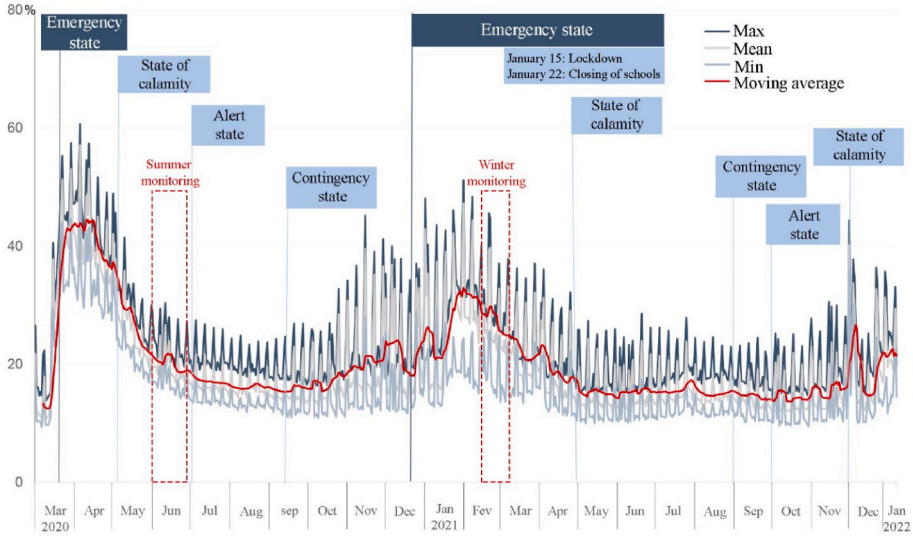

Fig. 2. Fraction of the population that "stayed at home" between March 1, 2020 and January 10, 2022, and the period of mobile monitoring. Adapted from INE (2021).

campaigns evaluated the external PM_{10} concentrations for the warm and cold periods in Bragança. Good correlations were obtained between the OPS and DustTrak (R^2 of 0.89 and 0.9 for the warm and cold period, respectively). The PM_{10} concentrations measured by the OPS were corrected based on the equations described in Fig. S3. Subsequently, the OPS data resulting from the first inter-comparison began to be corrected by the second equation (Fig. S4, Supplementary Material) obtained through the correlation of DustTrak and Gravimetric data. In the second stage of inter-comparison, DustTrak shows an excess of mass concentration in relation to the gravimetric method (cold period), by a factor of up to 1.82, in line with correction factors reported in other studies conducted in urban areas (Kingham et al., 2006; Wallace et al., 2011). PM_1 and $PM_{2.5}$ data were corrected based on PM_{10} concentrations. As we didn't have correlations for all size fractions, we used the ratios obtained between the initial concentrations of PM_1/PM_{10} and $PM_{2.5}/PM_{10}$ and multiplied by the concentrations of corrected PM_{10}, assuming that the proportions would be maintained between the segregated size fractions.

2.5. MPPD model and inhaled dose

The Multiple Path Particle Dosimetry model (MPPD version 3.04) was used to calculate three main deposition parameters in the human respiratory tract (HRT), namely, deposition fraction (DF), deposited mass rate (DMR), and clearance rate of inhaled PM (Anjilvel, 1995). The MPPD model software is freely available to the public (https://www.ara.com/mppd/) with a user-friendly interface and menu-driven selections. To simulate lung particle deposition, eight options are available: Stochastic lung, Age-specific Symmetric, Age-specific 5 lobe, Yeh-Schum Symmetric, Yeh-Schum 5 lobe, Weibel and Pacific Northwest National Laboratories (PNNL) Symmetric and PNNL Asymmetric models. Here, the Yeh-Schum 5 lobe model (Cassee et al., 1999) was adopted to estimate particle deposition in human respiratory regions in more detail, considering multiple paths, asymmetric lung geometry, airway size and respiratory parameters. The DF calculations are based on the deposition efficiency by several mechanisms (diffusion, impaction, and sedimentation) as a function of lung anatomy, tidal volume, breathing rate, mass median aerodynamic diameter (MMAD) and geometric standard deviation (GSD). The DMR shows the rate at which the mass of PM was deposited in a specific region. The clearance rate refers to the rate at which particles are eliminated from the lung in a two-step process: i) a rapid phase where clearance occurs in the TB region through mucociliary activity, and ii) a slow phase where particles are removed by alveolar macrophages in the P region. MMAD and GSD were calculated for PM_1, $PM_{2.5}$ and PM_{10} and for the different periods of the day and pandemic phases (Table 1).

A number of parameters were used as input variables for the MPPD to simulate the size-segregated deposition fraction (Table 2), considering the non-use of protective masks due to changes in respiratory rate patterns (Ciocan et al., 2020) and particle retention (Pacitto et al., 2019). The following assumptions were made for both genders when estimating DF: respiratory fraction of 0.5, unit density particles (1 g cm^{-3}), nasal breathing route and constant exposure. The inhaled dose was subsequently calculated using the DF provided by the MPPD model following equation (1) (Goel et al., 2018):

$$Dose(\mu g) = \sum PM_i * DF * t * VE \quad (1)$$

where PM_i is the median PM concentration of size fraction i (in μg m^{-3}) for each sampling period, t (min) is the exposure time, set up as 60 min to calculate the hourly dosage exposure to PM within the mobile sample range, and VE is the ventilation per minute (L min^{-1}). The VE was obtained from the literature, adopting the short-term exposure values (males and females combined) recommended by the USEPA (2011). A mean VE of 12.5 L min-1 was used to represent a light intensity walk for the age group from 21 to 81 years. All the particles were assumed to enter in the HRT through the nose. The selection of the nasal route was based on two main reasons: (1) mouth breathers deposit more PM in the respiratory system, especially for the extrathoracic region than those with nasal breathing (Lippmann et al., 1980); (2) It was assumed that the study population (pedestrians) were walking at light intensity and breathing spontaneously through the nose. Bragança is characterised by an inverted age pyramid, with an overwhelming majority of the population in adulthood. Thus, in the modelling assessment only adults of any gender were considered. It should be noted that the ratio between the number of female and male inhabitants in the municipality is close to 1.

Table 1
MMAD and GSD values used in the MPPD model simulations.

Period	MMAD (μm)			GSD		
	State of Calamity					
	PM_1	$PM_{2.5}$	PM_{10}	PM_1	$PM_{2.5}$	PM_{10}
morning	0.43	1.38	6.34	2.42	2.22	2.01
afternoon	0.49	1.65	6.33	2.41	2.23	2.02
State of Emergency						
Morning	0.51	1.76	4.82	2.22	2.41	2.18
Afternoon	0.39	0.63	2.10	3.59	3.38	4.34

Table 2
Input parameters for the MPPD model.

Parameters		Options/Values	
		Adult Male	Adult Female
Airway Morphometry	Species	Human	
	Model	Yeh/Schum 5-Lobe	
	FRC (ml)[a]	3300	2680
	URT volume (ml)[b]	50	40
	Density (g cm^{-3})	1	1
Particle Properties	Aspect ratio	1	1
	Diameter (μm)	MMAD	MMAD
	Particle distribution	Single	Single
	MMAD	Calculated	Calculated
	GSD	Calculated	Calculated
	Exposure condition	Constant exposure	
Exposure Scenario	Aerosol concentration (μg m^{-3})	PM_1, $PM_{2.5}$ and PM_{10}	
	Breathing frequency (min^{-1})[c]	20	21
	Tidal volume (ml)[d]	1250	992
	Inspiratory fraction	0.5	0.5
	Breathing scenario	Nasal	Nasal

[a] FRC: functional residual capacity.
[b] URT: upper respiratory tract.
[c] (ICRP, 1994).
[d] (Brown et al., 2013).

2.6. Ancillary data

During the study period, meteorological data (air temperature, relative humidity, wind speed and direction) were collected continuously at 10-min rate with a portable meteorological station installed close to the industrial area (Fig. 1).

Regional pollution, such as wildfire smoke, can also contribute to PM concentrations in Portugal and Spain (Rigo et al., 2017). As PM background measurements were not available during the study period, the location of fire foci (http://effis.jrc.ec.europa.eu/) were combined with air mass backward trajectories to identify possible long-range transport events. In this study, six-day backward trajectories were calculated using the Hybrid Single-Particle Lagrangian Integrated Trajectory (HYSPLIT 4.0) model (Rolph et al., 2017) from the National Oceanic and Atmospheric Administration (NOAA), arriving at Bragança, 100 m above ground level, using a Global Forecast System Reanalysis (0.25°, global).

3. Results and discussion

3.1. General description

The meteorological conditions in the two sampling periods were clearly distinct, with mean air temperatures of 20.7 °C and 10.7 °C, mean relative humidity of 49% and 67% and mean wind speeds of 2.5 m s^{-1} and 1.2 m s^{-1} in the 1st (calamity) and 2nd (emergency) periods, respectively. Northwestly and southeastly winds prevailed in the 1st and 2nd periods, respectively. The fleet composition was the same in the two periods, largely dominated by light-duty vehicles (95.5% cars and 1.5% motorcycles), whilst heavy-duty vehicles represented a share of 2.5% for trucks and 0.5% for buses (Table S4 Supplementary Material). However, a 18% reduction was observed in the total number of vehicles from the 1st to the 2nd period, with heavy vehicles showing the highest percentage reduction (85%). The combined fire spots and backward trajectories showed that during the entire sampling period, the city was not affected by the long-range transport of smoke from forest fires (Fig. S5, Supplementary Material). Thus, it was assumed that the air pollution in the study area was mainly due to local sources.

3.2. Changes in particulate matter concentrations

In general, about 7-, 6-, and 5-fold increases in PM_1, $PM_{2.5}$, and PM_{10} were observed during the 2nd period compared to the 1st (Fig. 3). Although wood consumption for residential heating was not quantified, the greater increase in PM_1 in relation to the other fractions can be most likely attributed to residential wood combustion, given the numerous voice records reporting "smell of smoke", "chimneys emitting smoke" and "visibility reduced by smoke". The lowest mean PM concentrations were observed in the 1st period ($PM_1 = 2.33 \pm 1.61$ μg m^{-3}; $PM_{2.5} = 5.15 \pm 2.77$ μg m^{-3}; $PM_{10} = 23.30 \pm 21.53$ μg m^{-3}), while the highest concentrations corresponded to the 2nd period ($PM_1 = 16.85 \pm 31.80$ μg m^{-3}; $PM_{2.5} = 30.92 \pm 31.93$ μg m^{-3}; $PM_{10} = 111.27 \pm 104.53$ μg m^{-3}). A greater variability in concentrations was observed during the 2nd period than in the 1st, as shown by the difference between the 5th and 95th percentiles. Besides meteorological factors, seasonal changes in activities may have affected these variabilities (e.g., use of firewood for residential heating), as there was an 18% reduction in the total number of vehicles from the 1st to the 2nd period (Table S4, Supplementary Material).

Sicard et al. (2020) quantified the effect of lockdown during the COVID-19 pandemic in four cities in Europe and one in China, finding reductions in PM_{10} concentrations during lockdown of 6% in Nice, 9% in Turin, 32% in Valencia and 49% in Wuhan, while they increased by just 2% in Rome. For $PM_{2.5}$, changes of −2.9%, +10.6%, −12.6%, −12.6% and −36.3% were observed in Nice, Rome, Turin, Valencia and Wuhan, respectively. Abatements in $PM_{2.5}$ and PM_{10} for urban stations showed different magnitudes, with a reduction of around 8% in Europe and 42% in the Chinese city, due to increases in PM emissions in the residential sector, offsetting the effect of the reductions in the road traffic and fuel burning in commercial buildings.

In the most populous cities, such as Lisbon, the reductions in PM concentrations were more evident, with a decrease of approximately 43% (Rodríguez-Urrego and Rodríguez-Urrego, 2020). The results of the present study show that, despite the reductions in mobility and primary emissions from road traffic and industries during the 2nd period, mean PM concentrations remained high in Bragança when compared to the 1st period, at least during the sampling campaigns. With tighter restrictions imposed by local authorities, more people stayed at home during the 2nd period, increasing the likelihood of using firewood for space heating.

The median $PM_{2.5}/PM_{10}$ ratios were 0.21 and 0.30 for the 1st and 2nd periods, respectively. The lower value for the first period might be explained by construction activities observed in the central and upper part of the route (Figs. S5 and S6, Supplementary Material), contributing to the mineral dust load (coarse fraction). The higher ratio in the 2nd period might be due to the increase in fine particles, mainly from residential wood combustion. The role of residential biomass burning as the primary source of the finer PM fractions is evidenced and reinforced by the highest median values of the $PM_1/PM_{2.5}$ ratio found during the 1st (0.37) and 2nd period (0.44). High median values of $PM_1/PM_{2.5}$ (0.42) were found during the 1st period, related to unfavourable atmospheric conditions for the dispersion of pollutants (wind speed <1.6 m s^{-1}), while the highest median ratios ($PM_1/PM_{2.5} = 0.95$) were found near residential areas during the 2nd period.

3.3. Spatio-temporal characteristics of PM concentrations

The median spatial distributions of PM_1, $PM_{2.5}$, and PM_{10} are summarised in Fig. 4 (1st period) and Fig. 5 (2nd period). PM showed marked seasonal variability, with higher concentrations occurring during the 2nd period when compared to the warm season ($P < 0.05$). The concentrations in the 1st period were markedly higher in the morning than in the afternoon. This result can be explained by two main factors: 1) lower mixing height in the morning and lower wind speeds (mean: 1.86 m s^{-1}) compared to the afternoon (mean: 2.88 m s^{-1}), resulting in weaker dispersion; 2) more efficient formation of secondary fine

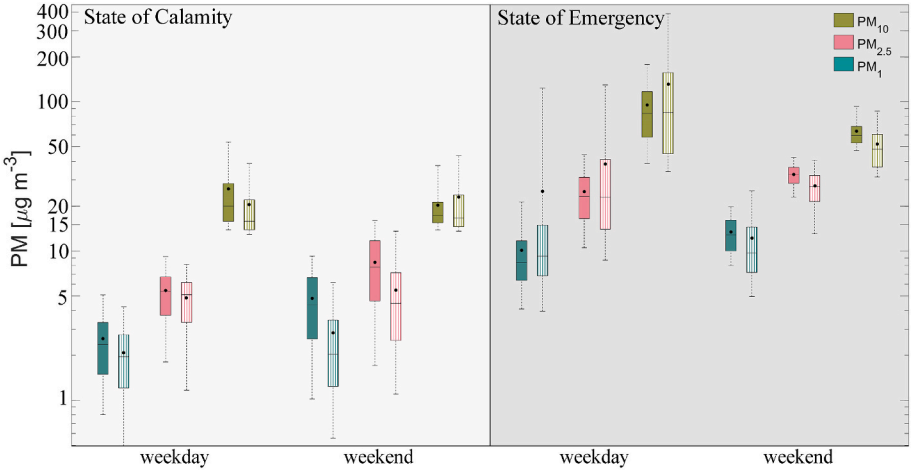

Fig. 3. - Boxplots of PM_1, $PM_{2.5}$ and PM_{10} concentrations on weekdays and weekends, morning (solid boxplots) and afternoon (boxplots with stripes) split per contingency phases of COVID-19. The box represents the interquartile range, whereas the upper and lower whiskers indicate the 95th and 5th percentiles, respectively. The median value is indicated by the line across the box, and the black circle represents the mean.

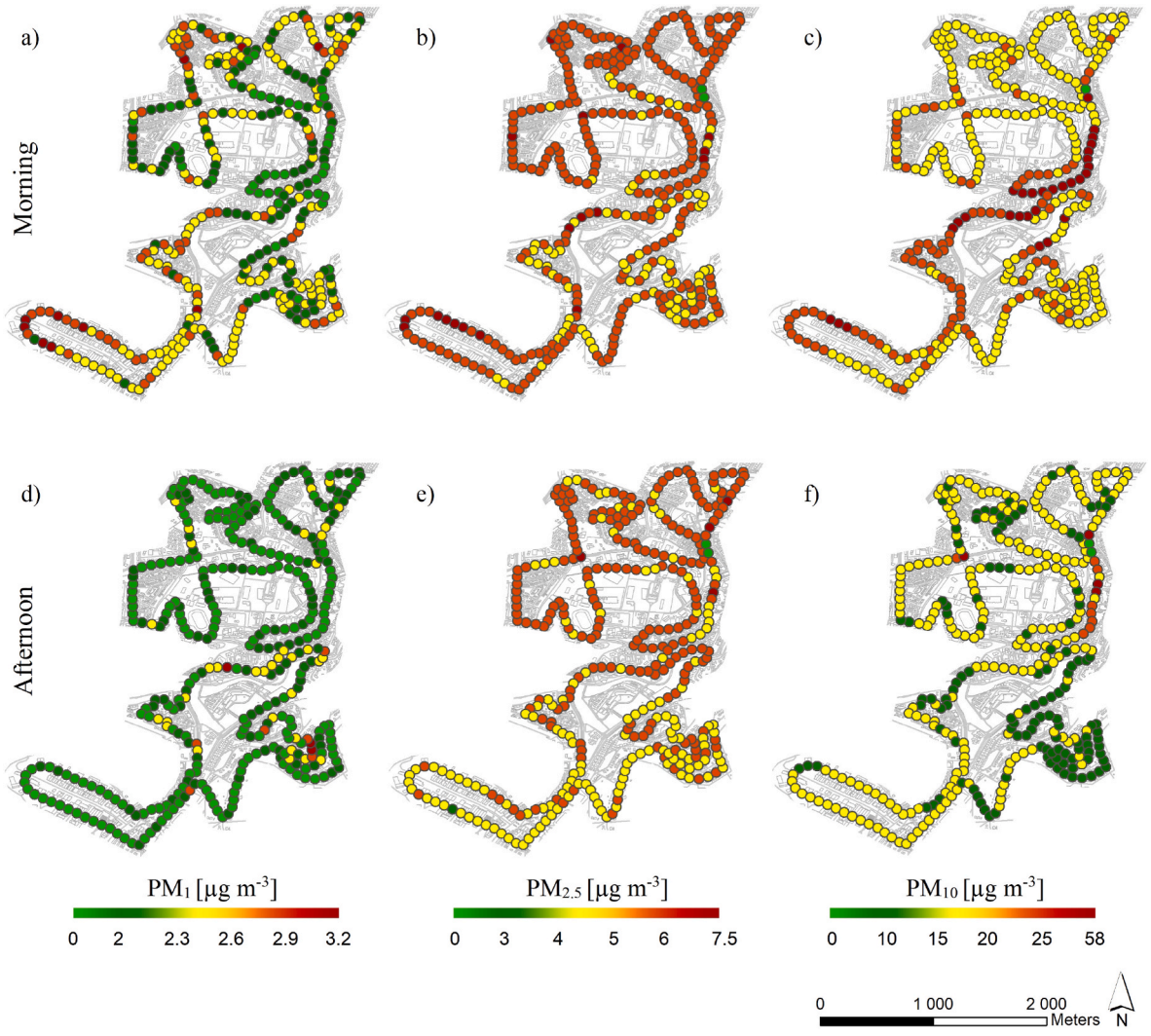

Fig. 4. Spatial distribution of median PM_1, $PM_{2.5}$, and PM_{10} concentrations in the state of calamity (May 30 to June 21, 2020) split by morning (a,b,c) and afternoon (d,e,f) periods for weekdays.

particles during the afternoon, due to higher temperatures and more photochemical activity (Wang et al., 2016). On the other hand, PM concentrations during the 2nd period showed higher values in the afternoon than in the morning, suggesting an increase in domestic emissions. Assuming that non-essential business (such as restaurants, coffee shop, and shopping mall) emissions decreased in the 2nd period due to the lockdown, this suggests that firewood burning outweighed this effect and contributed to the increase in PM concentrations. However, this hypothesis requires further investigations to better understand this behaviour.

In general, the highest PM concentrations in the 1st period occurred in the central part of the monitored area, where construction activities were taking place (e.g., main avenue of the city), reaching median PM_{10} values up to 57 µg m^{-3}, while the lowest concentrations (PM_1 = 1.05 µg m^{-3}; $PM_{2.5}$ = 3.03 µg m^{-3}; PM_{10} = 13.71 µg m^{-3}) were registered in the vicinity of open areas and green spaces. The 2nd period showed the lowest median concentrations (PM_1 = 3.43 µg m^{-3}; $PM_{2.5}$ = 11.47 µg m^{-3}; PM_{10} = 50.57 µg m^{-3}) in areas further away from residential neighbourhoods, while the highest median concentrations (PM_1 = 24.19 µg m^{-3}; $PM_{2.5}$ = 49.35 µg m^{-3}; PM_{10} = 236.55 µg m^{-3}) were recorded in areas where the highest population densities are observed.

3.4. PM deposition fractions

With respect to total deposition fractions (DF_{total} = DF_{head} + $DF_{tracheobronchial}$ + $DF_{pulmonay}$), PM_{10} represented the largest HRT inhaled deposition (65–97%), followed by $PM_{2.5}$ (46–68%) and PM_1 (32–40%), as shown in Table 3. The deposition fractions for $PM_{2.5}$ and PM_{10} showed a similar pattern: H > TB > P, while PM_1 presented higher values of deposition for the P region in relation to TB: H > P > TB.

The highest DFs for PM_{10} were found during the 1st period, while for the finest modes ($PM_{2.5}$ and PM_1), were higher during the 2nd period. This is likely due to a larger contribution of road dust resuspension to the coarse mode during the 1st period (PM_{10} with MMAD = 7.33 µm), while for the 2nd period, residential wood combustion emissions contributed to the increase of smaller particles (PM_{10} with MMAD = 3.01 µm). As for the region-specific deposition, PM sizes deposited in the H, TB and P varied over a noticeable range: head PM_{10} (56–92%) > $PM_{2.5}$ (31–57%) > PM_1 (17–23%), tracheobronchial PM_1 (4–5%) > $PM_{2.5}$ (3–4%) > PM_{10} (1–3%), and pulmonary PM_1 (9–12%) > $PM_{2.5}$ (8–11%) > PM_{10} (4–6%). In summary, PM_{10} was mostly deposited in the upper region of the respiratory system, while the finest size fractions penetrated into deeper airways. This result agrees with those documented by other authors (Amoatey et al., 2022; Behera et al., 2015; Manojkumar et al., 2019). For PM_{10}, the behaviour is related to the deposition mechanisms involved (impact and sedimentation) in the upper airways, while for

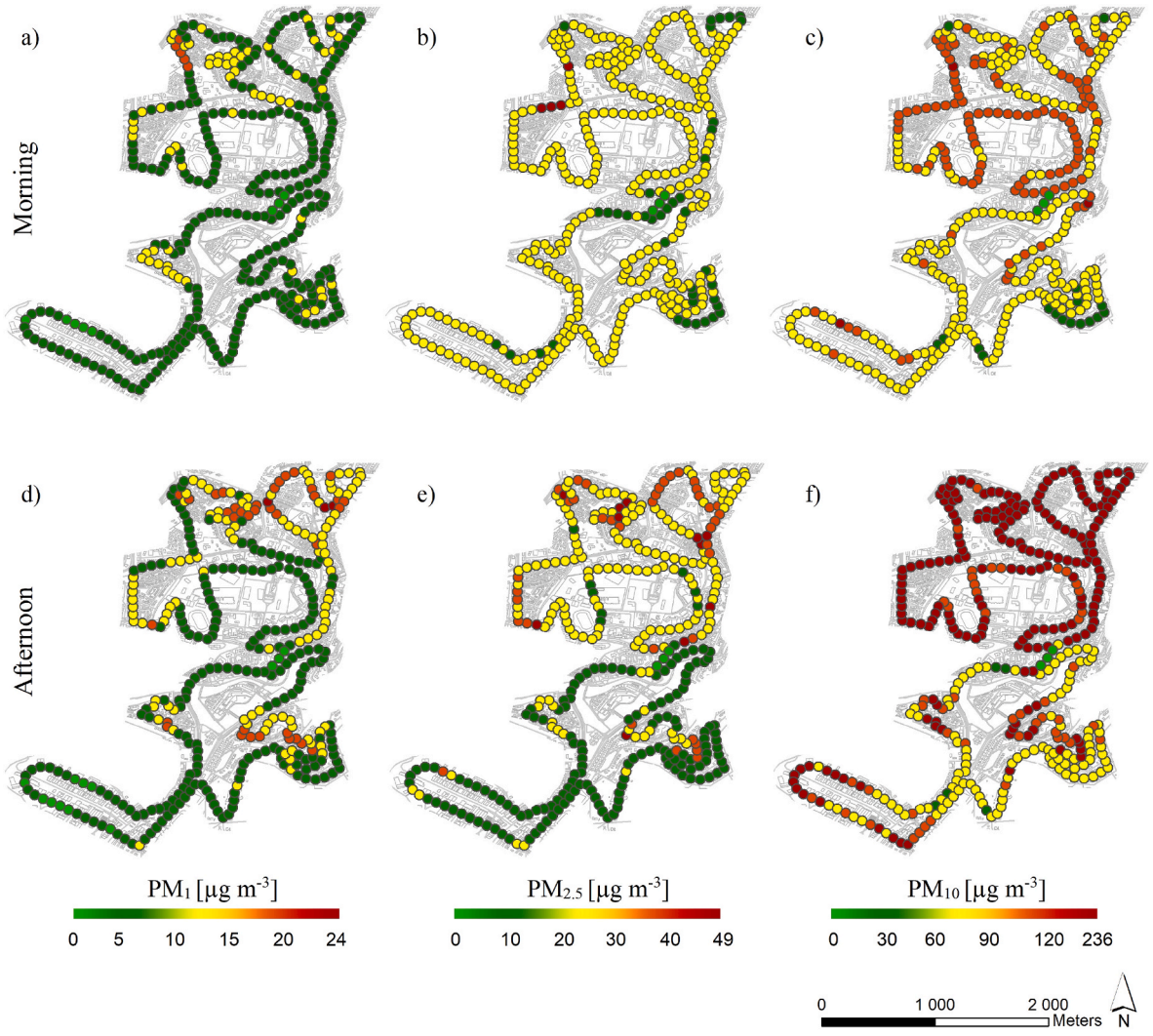

Fig. 5. Spatial distribution of median PM_1, $PM_{2.5}$, and PM_{10} concentrations in the state of emergency (February 15 to March 07, 2021) split by morning (a,b,c) and afternoon (d,e,f) periods for weekdays.

Table 3
Total and region-specific deposition fractions of PM_1, $PM_{2.5}$ and PM_{10} for male and female.

	Gender	**PM_1**				$PM_{2.5}$				PM_{10}			
		Total	H	TB	P	Total	H	TB	P	Total	H	TB	P
State of calamity													
Morning	Male	0.33	0.19	0.05	0.09	0.62	0.51	0.03	0.08	0.97	0.92	0.01	0.04
	Female	0.32	0.17	0.05	0.10	0.59	0.47	0.03	0.09	0.96	0.90	0.02	0.05
Afternoon	Male	0.35	0.21	0.04	0.09	0.67	0.56	0.03	0.08	0.97	0.91	0.01	0.04
	Female	0.33	0.19	0.04	0.10	0.65	0.53	0.03	0.09	0.96	0.90	0.02	0.04
State of emergency													
Morning	Male	0.34	0.21	0.04	0.09	0.68	0.57	0.03	0.08	0.93	0.86	0.02	0.05
	Female	0.33	0.19	0.04	0.09	0.66	0.54	0.03	0.08	0.92	0.84	0.02	0.06
Afternoon	Male	0.40	0.23	0.05	0.12	0.48	0.33	0.04	0.10	0.66	0.58	0.03	0.05
	Female	0.39	0.21	0.05	0.12	0.46	0.31	0.04	0.11	0.65	0.56	0.03	0.06

$PM_{2.5}$ and PM_1, the deposition is controlled by Brownian diffusion, reaching deeper airways. It was observed that differences based on population gender were small to negligible. Despite all pollutants having a similar behaviour, the total estimated DFs for males were slightly higher than for females in the different periods. This result is consistent with the findings by other studies (Hussein et al., 2013; Lv et al., 2021; Madureira et al., 2020; Manojkumar et al., 2019).

3.5. Mass rate deposition

For both genders, total DMR showed notable differences between measurements conducted in the 1st and 2nd periods. During the 2nd period, the total DMR reached values of up to 1.95 µg min^{-1} for PM_{10}, 0.39 µg min^{-1} for $PM_{2.5}$ and 0.09 µg min^{-1} for PM_1, being about 4 times higher than the values found for the 1st period (Tables S1 and S2,

Supplementary Material), in line with the high PM concentrations recorded during the 1st and 2nd periods. Furthermore, regardless of PM size, the total and regional mean DMR was higher for male than for female (12% PM_1, 11% $PM_{2.5}$ and 10% PM_{10}), due to the higher DFs calculated for males. Higher DMR values were observed during the afternoon of the 2nd period for P region, with regional lung deposition values for PM_1 (female = 0.23 μg min^{-1}; male = 0.27 μg min^{-1}) being higher than total DMR values for PM_1 (female = 0.15 μg min^{-1}; male = 0.19 μg min^{-1} during the 1st period, which also suggests the large contribution of firewood combustion to the emission of small particles. This result confirmed that the afternoon during the cold season had more harmful impacts on human health than any other period.

3.6. PM doses

For the 2nd period, the total dose showed a tendency for both genders, with PM_1 highest dose during the afternoon, whereas $PM_{2.5}$ and PM_{10} doses were highest in the morning period (see Fig. 6). The MMAD results for PM_1 during the 2nd period ($MMAD_{morning}$ = 0.51 μm, $MMAD_{afternoon}$ = 0.39 μm) reinforce the importance of particle size for regional deposition. Considering the dose deposited per region, the largest fraction of the total deposited dose was observed in the H (53–94%) and P (4–32%) regions, compared with the TB region (1–15%). It was estimated that PM_{10} contributed 95% of the dose in the head region, while PM_1 was pointed out as the main contributor to the doses experienced in the TB and P regions, with 28% and 24%, respectively. Similar findings of PM_{10} doses for the H region were observed in other studies, with contributions up to 98% (Gupta and Elumalai, 2017; Lv et al., 2021). As noted for the previous calculations by the model, the dose for all PM fractions followed the same tendency, with higher doses for males compared to females. The deposition doses in the winter period for males (females) were 4.1 (3.8), 3.9 (3.7), 4.5 (4.1) times higher in relation to the deposition doses found in the summer for PM_{10}, $PM_{2.5}$ and PM_1, respectively. Based on the results of this study, it is clear that seasonality is a decisive factor for population exposure and dose. This implies that the health effect of increasing biomass consumption during the winter period may be more significant for men than for women ($P < 0.05$).

3.7. Clearance of PM from the tracheobronchial and alveolar regions

The clearance of PM deposition in the TB and P regions was evaluated for the males in cold period, considering the higher vulnerability calculated to this gender and the doses for the 2nd period as the most critical scenario. The results of PM clearance in the different regions of the HRT are displayed in Fig. 7. For all PM fractions, a larger clearance was found in the TB region compared to the alveolar region. Note that the TB region presents a high rate of clearance in the first hours and becomes low in the later stages, whereas the clearance in the alveolar region is low and constant during the process. The particles deposited in TB have a high initial clearance rate due to mucociliary activity, whose glands secrete mucus to eliminate the deposited PM, via coughing and ciliary movements (Walsh et al., 2011). The lower clearance rate for the P region is attributed to the processes of phagocytosis and lymphatic transport, mechanisms of slow nature for PM clearance (Lippmann et al., 1980; Manigrasso et al., 2017). Removal time may favour the accumulation of PM in these regions, and faster removal decreases the time available to cause interactions and direct tissue damage (Pauluhn, 2011).

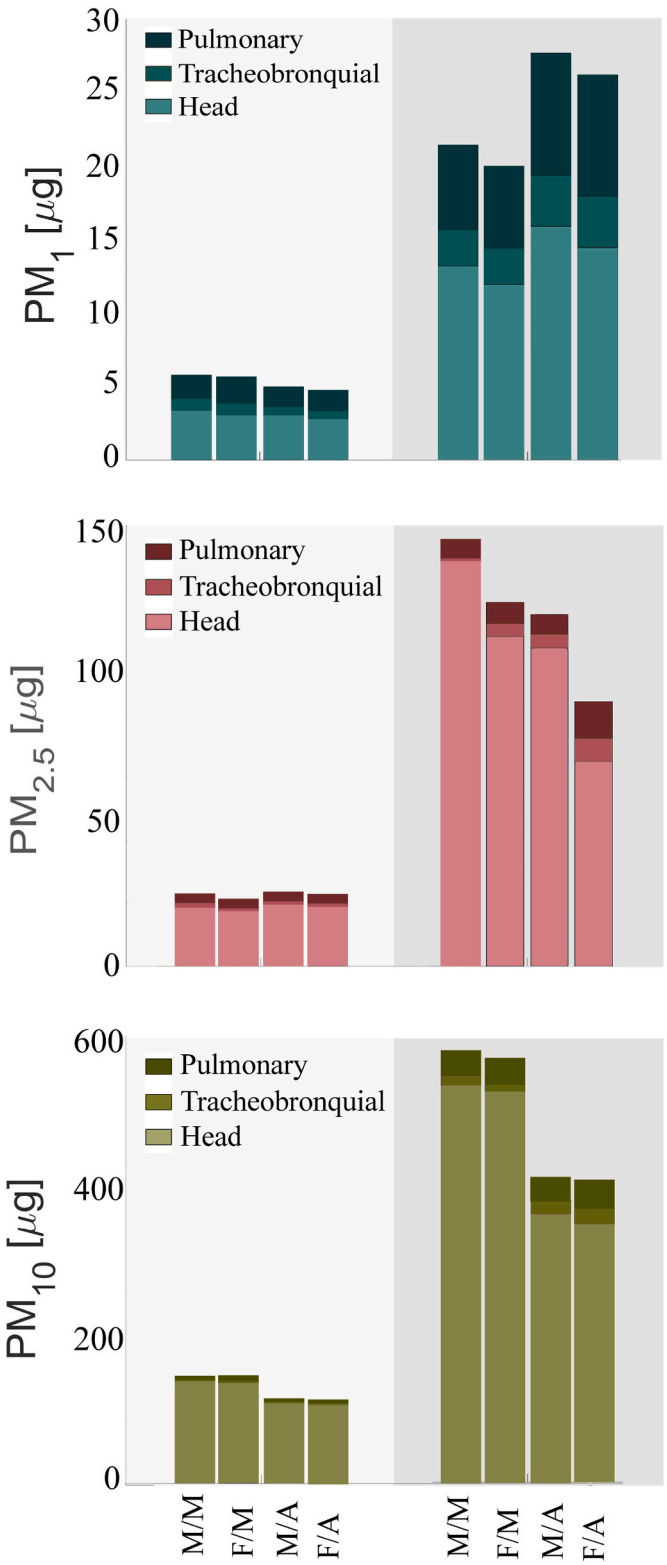

Fig. 6. Deposition doses of PM_1, $PM_{2.5}$ and PM_{10} in specific regions (head, tracheobronquial and pulmonary) split per gender, period of the day, and contingency phases of COVID-19. M/M = male/morning; F/M = female/morning; M/A = male/afternoon; F/A = female/afternoon.

4. Study limitations

Some aspects that may have interfered with the data collection and interpretation must be highlighted: i) the study started spontaneously in an opportunistic period, when restrictive measures were implemented due to the COVID-19 pandemic, reducing certain human activities and, thus, changing typical emission patterns, ii) calculations of PM deposition in the respiratory tract were only performed for morning and afternoon periods, and iii) the spatial representativeness of the study in is limited. Thus, to improve the exposure assessment in future works,

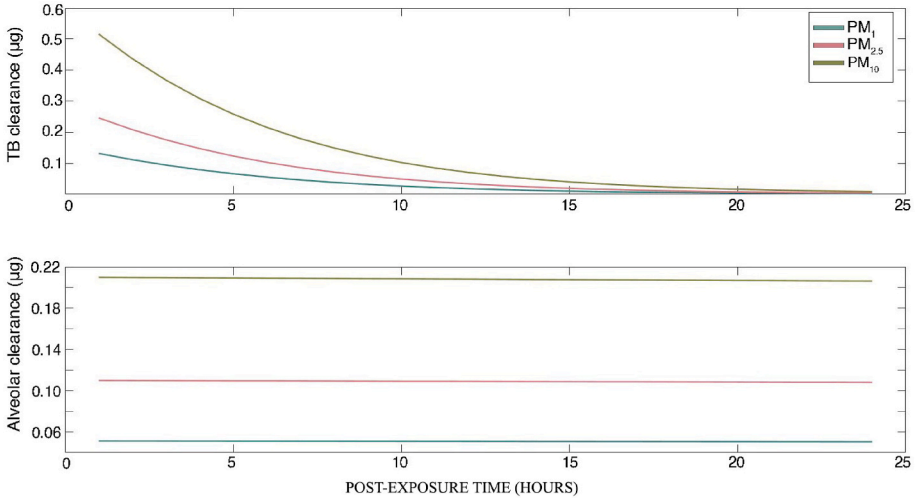

Fig. 7. Clearance in TB and alveolar regions in the post exposure period.

different periods should be considered, covering other urban areas to identify new patterns and using an instrument capable of measuring a full range of particles (ultrafine to coarse particles).

5. Summary and conclusions

The PM fractions (PM_1, $PM_{2.5}$ and PM_{10}) showed higher concentrations in the 2nd period compared to the 1st period, which can be attributed to meteorological factors such as the lower wind speed and higher atmospheric stability favouring the accumulation of pollutants, and anthropogenic factors, such as residential wood consumption for space heating during the winter season. Furthermore, high concentrations of PM_{10} and $PM_{2.5}$ were found during the 1st period, associated with resuspension of road and construction site dust. Regarding the 2nd period, the high levels of PM in all fractions are linked to biomass burning, since it was a period with low urban traffic and reduced industrial activities. Through the MPPD dosimetry model, it was observed that PM_{10} was the fraction that most contributed to the total deposition, followed by $PM_{2.5}$ and PM_1. The highest deposition values for the head region were attributed to PM_{10}, while the deposition in the tracheobronchial and pulmonary regions was dominated by PM_1. Moreover, higher PM deposited doses were observed for males compared to females. The mass deposition rate was also higher in males, whose values were higher during the 2nd period. The clearance rate of PM deposited in the post-exposure period is initially fast in the TB region, but it loses intensity with the passing of hours, while in the alveolar region, clearance is very slow throughout the process. In general, the variability of the PM deposition doses can be associated with the high spatio-temporal variability observed in exposure concentrations, travel time and particle size. As future work, it is recommended a multi-pollutant assessment to get a more complete overview of the impact on the air quality. Because the reduction in mobility was not sufficient to reduce the atmospheric PM levels, an accurate source distribution is required. In particular, emissions from residential wood burning should be better characterised, considering the regional specificities of biofuels and appliances to better understand their health effects and implications for the atmospheric chemistry, as well as to design awareness campaigns and regulatory measures.

Credit author contribution statement

Yago A. Cipoli: Conceptualization, Formal analysis, Investigation, Methodology, Writing – original draft & Editing. **Admir C. Targino**: Writing – original draft & review, Conceptualization, Methodology, Supervision. **Patricia Krecl**: Writing – original draft & review; Conceptualization, Methodology. **Leonardo C. Furst**: Data curation. Célia A. Alves: Writing – review & editing; **Manuel Feliciano**: Supervision, Conceptualization, Writing – review & editing, Funding acquisition.

Declaration of competing interest

The authors declare that they have no known competing financial interests or personal relationships that could have appeared to influence the work reported in this paper.

Acknowledgments

Yago A. Cipoli acknowledges the Portuguese Foundation of Science and Technology (FCT) for the PhD scholarship (SFRH/BD/04992/2021). The authors thank the Base Funding UIDB/00690/2020 of the Centro de Investigação de Montanha (CIMO) - funded by national funds through FCT/MCTES (PIDDAC), and the financial support to CESAM by FCT/MCTES (UIDP/50017/2020, UIDB/50017/2020 and LAP/0094/2020).

Appendix A. Supplementary data

Supplementary data to this article can be found online at https://doi.org/10.1016/j.apr.2022.101512.

References

Adam, M.G., Tran, P.T.M., Balasubramanian, R., 2021. Air quality changes in cities during the COVID-19 lockdown: a critical review. Atmos. Res. 264, 105823 https://doi.org/10.1016/J.ATMOSRES.2021.105823.

Amoatey, P., Omidvarborna, H., Al-Jabri, K., Al-Harthy, I., Baawain, M.S., Al-Mamun, A., 2022. Deposition modeling of airborne particulate matter on human respiratory tract during winter seasons in arid-urban environment. Aerosol Sci. Eng. 6, 71–85. https://doi.org/10.1007/S41810-021-00125-2.

Anjilvel, S., 1995. A multiple-path model of particle deposition in the rat lung. Fund. Appl. Toxicol. 28, 41–50. https://doi.org/10.1006/FAAT.1995.1144.

Azevedo, J.C., Ferreira, M.C., Nunes, L.F., Feliciano, M., 2016. What drives consumption of wood energy in the residen-tial sector of small cities in Europe and how that can affect forest resources locally? The case of Bragança. Portugal. Int. For. Rev. 18, 1. https://doi.org/10.1505/146554816818206177.

Behera, S.N., Betha, R., Huang, X., Balasubramanian, R., 2015. Characterization and estimation of human airway deposition of size-resolved particulate-bound trace elements during a recent haze episode in Southeast Asia. Environ. Sci. Pollut. Res. 22, 4265–4280. https://doi.org/10.1007/s11356-014-3645-6.

Brown, J.S., Gordon, T., Price, O., Asgharian, B., 2013. Thoracic and respirable particle definitions for human health risk assessment. Part. Fibre Toxicol 10 (1), 1–12. https://doi.org/10.1186/1743-8977-10-12.

Caggiano, R., Sabia, S., Speranza, A., 2019. Trace elements and human health risks assessment of finer aerosol atmospheric particles (PM_1). Environ. Sci. Pollut. Res. 26, 36423–36433. https://doi.org/10.1007/S11356-019-06756-W.

Cassee, F., Freijer, J., Subramaniam, R., 1999. Development of a Model for Human and Rat Airway Particle Deposition: Implications for Risk Assessment, Report No. 624029001. National Institute of Public Health and Environment, Bilthoven, The Netherlands.

Chen, P., Bi, X., Zhang, J., Wu, J., Feng, Y., 2015. Assessment of heavy metal pollution characteristics and human health risk of exposure to ambient $PM_{2.5}$ in Tianjin, China. Particuology 20, 104–109. https://doi.org/10.1016/J.PARTIC.2014.04.020.

Ciocan, C., Marco, C., Donatella, F., Maria, L.P., Giacomo, G., Alessandro, G., Attilia, G., Canzio, R., 2020. mpact of wearing a surgical mask on respiratory function in view of a widespread use during COVID-19 outbreak. A case-series study. La Medicina del lavoro 111 (5), 354. https://doi.org/10.23749/MDL.V111I5.9766.

Collivignarelli, M.C., De Rose, C., Abbà, A., Baldi, M., Bertanza, G., Pedrazzani, R., Sorlini, S., Carnevale Miino, M., 2021. Analysis of lockdown for COVID-19 impact on NO_2 in London, Milan and Paris: what lesson can be learnt? Process Saf. Environ. Protect. 146, 952–960. https://doi.org/10.1016/J.PSEP.2020.12.029.

Dantas, L., Azevedo, J.C., Feliciano, M., 2019. O impacto da queima doméstica de biomassa lenhosa nos níveis de $PM_{2,5}$ na cidade de Bragança. Portugal. Rev. Ciências Agrárias 40, 282–290. https://doi.org/10.19084/RCA16191.

de Nazelle, A., Fruin, S., Westerdahl, D., Martinez, D., Ripoll, A., Kubesch, N., Nieuwenhuijsen, M., 2012. A travel mode comparison of commuters' exposures to air pollutants in Barcelona. Atmos. Environ. 59, 151–159. https://doi.org/10.1016/J.ATMOSENV.2012.05.013.

DRE, 2021. Portuguese legislation COVID-19. accessed 1.21.22. https://dre.pt/dre/geral/legislacao-covid-19.

Fernández, A.J., Sicard, M., Costa, M.J., Guerrero-Rascado, J.L., Gómez-Amo, J.L., Molero, F., Barragán, R., Basart, S., Bortoli, D., Bedoya-Velásquez, A.E., Utrillas, M. P., Salvador, P., Granados-Muñoz, M.J., Potes, M., Ortiz-Amezcua, P., Martínez-Lozano, J.A., Artiñano, B., Muñoz-Porcar, C., Salgado, R., Román, R., Rocadenbosch, F., Salgueiro, V., Benavent-Oltra, J.A., Rodríguez-Gómez, A., Alados-Arboledas, L., Comerón, A., Pujadas, M., 2019. Extreme, wintertime Saharan dust intrusion in the Iberian Peninsula: lidar monitoring and evaluation of dust forecast models during the February 2017 event. Atmos. Res. 228, 223–241. https://doi.org/10.1016/J.ATMOSRES.2019.06.007.

Goel, A., Izhar, S., Gupta, T., 2018. Study of environmental particle levels, its effects on lung deposition and relationship with human behaviour. Energy Environ. Sustain. 77–91. https://doi.org/10.1007/978-981-10-7332-8_4.

Goel, R., Gani, S., Guttikunda, S.K., Wilson, D., Tiwari, G., 2015. On-road $PM_{2.5}$ pollution exposure in multiple transport microenvironments in Delhi. Atmos. Environ. 123, 129–138. https://doi.org/10.1016/J.ATMOSENV.2015.10.037.

Gupta, S.K., Elumalai, S.P., 2017. Size-segregated particulate matter and its association with respiratory deposition doses among outdoor exercisers in Dhanbad City, India. J. Air Waste Manag. Assoc. 67, 1137–1145. https://doi.org/10.1080/10962247.2017.1344159.

Hassanvand, M.S., Naddafi, K., Faridi, S., Nabizadeh, R., Sowlat, M.H., Momeniha, F., Gholampour, A., Arhami, M., Kashani, H., Zare, A., Niazi, S., Rastkari, N., Nazmara, S., Ghani, M., Yunesian, M., 2015. Characterization of PAHs and metals in indoor/outdoor $PM_{10}/PM_{2.5}/PM_1$ in a retirement home and a school dormitory. Sci. Total Environ. 527–528, 100–110. https://doi.org/10.1016/J.SCITOTENV.2015.05.001.

Hussein, T., Löndahl, J., Paasonen, P., Koivisto, A.J., Petäjä, T., Hämeri, K., Kulmala, M., 2013. Modeling regional deposited dose of submicron aerosol particles. Sci. Total Environ. 458–460. https://doi.org/10.1016/J.SCITOTENV.2013.04.022, 140–149.

ICRP, 1994. Human Respiratory Tract Model for Radiological Protection. ICRP Publication 66, Ann., 24 (1–3).

INE, 2021. Indicators of the demographic context and territorial expression of the COVID-19 pandemic in Portugal. https://www.sgeconomia.gov.pt/noticias/ine-indicadores-de-contexto-para-a-pandemia-covid-19-em-portugal-dados-ate-10-de-maio-span-classnovo-novospan.aspx. (Accessed 30 July 2021).

Jasiński, R., Galant-Gołębiewska, M., Nowak, M., Kurtyka, K., Kurzawska, P., Maciejewska, M., Ginter, M., 2021. Emissions and concentrations of particulate matter in Poznan compared with other Polish and European cities. Atmosphere 12, 533. https://doi.org/10.3390/ATMOS12050533.

Jia, S., Zhang, Q., Sarkar, S., Mao, J., Hang, J., Chen, W., Wang, X., Yuan, L., Yang, L., Ye, G., Zhou, S., 2020. Size-segregated deposition of atmospheric elemental carbon (EC) in the human respiratory system: a case study of the Pearl River Delta, China. Sci. Total Environ. 708, 134932 https://doi.org/10.1016/J.SCITOTENV.2019.134932.

Jing, H., Li, Y.F., Zhao, J., Li, B., Sun, J., Chen, R., et al., 2014. Wide-range particle characterization and elemental concentration in Beijing aerosol during the 2013 Spring Festival. Environ. Pollut. 192, 204–211. https://doi.org/10.1016/j.envpol.2014.06.003.

Kaur, S., Nieuwenhuijsen, M.J., Colvile, R.N., 2005. Pedestrian exposure to air pollution along a major road in Central London, UK. Atmos. Environ. 39, 7307–7320. https://doi.org/10.1016/J.ATMOSENV.2005.09.008.

Kecorius, S., Madueño, L., Löndahl, J., Vallar, E., Galvez, M.C., Idolor, L.F., Gonzaga-Cayetano, M., Müller, T., Birmili, W., Wiedensohler, A., 2019. Respiratory tract deposition of inhaled roadside ultrafine refractory particles in a polluted megacity of South-East Asia. Sci. Total Environ. 663, 265–274. https://doi.org/10.1016/J.SCITOTENV.2019.01.338.

Kingham, S., Durand, M., Aberkane, T., Harrison, J., Wilson, J.G., Epton, M., 2006. Winter comparison of TEOM, MiniVol and DustTrak PM_{10} monitors in a woodsmoke environment. Atmos. Environ. 40 (2), 338–347. https://doi.org/10.1016/j.atmosenv.2005.09.042.

Krecl, P., Cipoli, Y.A., Targino, A.C., Castro, L.B., Gidhagen, L., Malucelli, F., Wolf, A., 2020a. Cyclists' exposure to air pollution under different traffic management strategies. Sci. Total Environ. 723, 138043 https://doi.org/10.1016/J.SCITOTENV.2020.138043.

Krecl, P., Cipoli, Y.A., Targino, A.C., Toloto, M. de O., Segersson, D., Parra, Á., Polezer, G., Godoi, R.H.M., Gidhagen, L., 2019. Modelling urban cyclists' exposure to black carbon particles using high spatiotemporal data: a statistical approach. Sci. Total Environ. 679, 115–125. https://doi.org/10.1016/J.SCITOTENV.2019.05.043.

Krecl, P., Targino, A.C., Oukawa, G.Y., Junior, R.P.C., 2020b. Drop in urban air pollution from COVID-19 pandemic: policy implications for the megacity of São Paulo. Environ. Pollut. 265, 114883 https://doi.org/10.1016/J.ENVPOL.2020.114883.

Lippmann, M., Yeates, D.B., Albert, R.E., 1980. Deposition, retention, and clearance of inhaled particles. Occup. Environ. Med. 37, 337–362. https://doi.org/10.1136/OEM.37.4.337.

Liu, L., Breitner, S., Schneider, A., Cyrys, J., Brüske, I., Franck, U., Schlink, U., Marian Leitte, A., Herbarth, O., Wiedensohler, A., Wehner, B., Pan, X., Wichmann, H.E., Peters, A., 2013. Size-fractioned particulate air pollution and cardiovascular emergency room visits in Beijing, China. Environ. Res. 121, 52–63. https://doi.org/10.1016/J.ENVRES.2012.10.009.

Lv, H., Li, H., Qiu, Z., Zhang, F., Song, J., 2021. Assessment of pedestrian exposure and deposition of PM10, PM2.5 and ultrafine particles at an urban roadside: a case study of Xi'an, China. Atmos. Pollut. Res. 12, 112–121. https://doi.org/10.1016/J.APR.2021.02.018.

Madureira, J., Slezakova, K., Silva, A.I., Lage, B., Mendes, A., Aguiar, L., Pereira, M.C., Teixeira, J.P., Costa, C., 2020. Assessment of indoor air exposure at residential homes: inhalation dose and lung deposition of PM_{10}, $PM_{2.5}$ and ultrafine particles among newborn children and their mothers. Sci. Total Environ. 717, 137293 https://doi.org/10.1016/J.SCITOTENV.2020.137293.

Manigrasso, M., Natale, C., Vitali, M., Protano, C., Avino, P., 2017. Pedestrians in traffic environments: ultrafine particle respiratory doses. Int. J. Environ. Res. Publ. Health 14, 288. https://doi.org/10.3390/IJERPH14030288.

Manojkumar, N., Srimuruganandam, B., Shiva Nagendra, S.M., 2019. Application of multiple-path particle dosimetry model for quantifying age specified deposition of particulate matter in human airway. Ecotoxicol. Environ. Saf. 168, 241–248. https://doi.org/10.1016/J.ECOENV.2018.10.091.

McNabola, A., Broderick, B.M., Gill, L.W., 2008. Relative exposure to fine particulate matter and VOCs between transport microenvironments in Dublin: personal exposure and uptake. Atmos. Environ. 42, 6496–6512. https://doi.org/10.1016/J.ATMOSENV.2008.04.015.

Menon, J.S., Nagendra, S.M.S., 2018. Personal exposure to fine particulate matter concentrations in central business district of a tropical coastal city. J. Air Waste Manag. Assoc. 68, 415–429. https://doi.org/10.1080/10962247.2017.1407837.

Menut, L., Bessagnet, B., Siour, G., Mailler, S., Pennel, R., Cholakian, A., 2020. Impact of lockdown measures to combat Covid-19 on air quality over western Europe. Sci. Total Environ. 741, 140426 https://doi.org/10.1016/J.SCITOTENV.2020.140426.

Nazarenko, Y., Pal, D., Ariya, P.A., 2021. Air quality standards for the concentration of particulate matter 2.5, global descriptive analysis. Bull. World Health Organ. 99, 125. https://doi.org/10.2471/BLT.19.245704.

Nie, D., Shen, F., Wang, J., Ma, X., Li, Z., Ge, P., Ou, Y., Jiang, Y., Chen, Meijuan, Chen, Mindong, Wang, T., Ge, X., 2021. Changes of air quality and its associated health and economic burden in 31 provincial capital cities in China during COVID-19 pandemic. Atmos. Res. 249, 105328 https://doi.org/10.1016/J.ATMOSRES.2020.105328.

Pacitto, A., Amato, F., Salmatonidis, A., Moreno, T., Alastuey, A., Reche, C., Buonanno, G., Benito, C., Querol, X., 2019. Effectiveness of commercial face masks to reduce personal PM exposure. Sci. total. Environ. 650, 1582–1590. https://doi.org/10.1016/J.SCITOTENV.2018.09.109.

Pattinson, W., Kingham, S., Longley, I., Salmond, J., 2017. Potential pollution exposure reductions from small-distance bicycle lane separations. J. Transport Health 4, 40–52. https://doi.org/10.1016/J.JTH.2016.10.002.

Pauluhn, J., 2011. Poorly soluble particulates: searching for a unifying denominator of nanoparticles and fine particles for DNEL estimation. Toxicology 279, 176–188. https://doi.org/10.1016/J.TOX.2010.10.009.

Peel, M.C., Finlayson, B.L., Mcmahon, T.A., 2007. Hydrology and earth system sciences updated world map of the köppen-geiger climate classification. Hydrol. Earth Syst. Sci. 11, 1633–1644.

Pereira, S., Wagner, F., Silva, A.M., 2008. Scattering properties and mass concentration of local and long-range transported aerosols over the South Western Iberia Peninsula. Atmos. Environ. 42, 7623–7631. https://doi.org/10.1016/J.ATMOSENV.2008.06.008.

Pordata, 2021. Pordata - municipalities database. accessed 3.21.22. https://www.pordata.pt/Municipios.

Prabhu, V., Gupta, S.K., Madhwal, S., Shridhar, V., 2019. Exposure to atmospheric particulates and associated respirable deposition dose to street vendors at the residential and commercial sites in Dehradun City. Saf. Health Work 10, 237–244. https://doi.org/10.1016/J.SHAW.2019.01.005.

Querol, X., Massagué, J., Alastuey, A., Moreno, T., Gangoiti, G., Mantilla, E., Duéguez, J. J., Escudero, M., Monfort, E., Pérez García-Pando, C., Petetin, H., Jorba, O., Vázquez, V., de la Rosa, J., Campos, A., Muñóz, M., Monge, S., Hervás, M., Javato, R., Cornide, M.J., 2021. Lessons from the COVID-19 air pollution decrease in Spain: now what? Sci. Total Environ. 779, 146380 https://doi.org/10.1016/J.SCITOTENV.2021.146380.

Quiros, D.C., Lee, E.S., Wang, R., Zhu, Y., 2013. Ultrafine particle exposures while walking, cycling, and driving along an urban residential roadway. Atmos. Environ. 73, 185–194. https://doi.org/10.1016/J.ATMOSENV.2013.03.027.

Ramachandran, S., Cherian, R., 2008. Regional and seasonal variations in aerosol optical characteristics and their frequency distributions over India during 2001–2005. J Geophysical Res: Atmospheres, 113. https://doi.org/10.1029/2007JD008560.

Rigo, D. de, Libertà, G., Durrant, T.H., Vivancos, T.A., San-Miguel-Ayanz, J., 2017. Forest Fire Danger Extremes in Europe under Climate Change: Variability and Uncertainty. Publication Office of the European Union. Publications Office of the European Union. https://doi.org/10.2760/13180.

Rodríguez-Urrego, D., Rodríguez-Urrego, L., 2020. Air quality during the COVID-19: $PM_{2.5}$ analysis in the 50 most polluted capital cities in the world. Environ. Pollut. 266, 115042 https://doi.org/10.1016/J.ENVPOL.2020.115042.

Rolph, G., Stein, A., Stunder, B., 2017. Real-time environmental applications and display sYstem: ready. Environ. Model. Software 95, 210–228. https://doi.org/10.1016/J.ENVSOFT.2017.06.025.

Russo, A., Sousa, P.M., Durão, R.M., Ramos, A.M., Salvador, P., Linares, C., Díaz, J., Trigo, R.M., 2020. Saharan dust intrusions in the Iberian Peninsula: predominant synoptic conditions. Sci. Total Environ. 717, 137041 https://doi.org/10.1016/J.SCITOTENV.2020.137041.

Samek, L., Stegowski, Z., Styszko, K., Furman, L., Fiedor, J., 2018. Seasonal contribution of assessed sources to submicron and fine particulate matter in a Central European urban area. Environ. Pollut. 241, 406–411. https://doi.org/10.1016/J.ENVPOL.2018.05.082.

Sicard, P., De Marco, A., Agathokleous, E., Feng, Z., Xu, X., Paoletti, E., Rodriguez, J.J.D., Calatayud, V., 2020. Amplified ozone pollution in cities during the COVID-19 lockdown. Sci. Total Environ. 735, 139542 https://doi.org/10.1016/J.SCITOTENV.2020.139542.

Sokhi, R.S., Singh, V., Querol, X., Finardi, S., Targino, A.C., Andrade, M. de F., Pavlovic, R., Garland, R.M., Massagué, J., Kong, S., Baklanov, A., Ren, L., Tarasova, O., Carmichael, G., Peuch, V.H., Anand, V., Arbilla, G., Badali, K., Beig, G., Belalcazar, L.C., Bolignano, A., Brimblecombe, P., Camacho, P., Casallas, A., Charland, J.P., Choi, J., Chourdakis, E., Coll, I., Collins, M., Cyrys, J., da Silva, C.M., Di Giosa, A.D., Di Leo, A., Ferro, C., Gavidia-Calderon, M., Gayen, A., Ginzburg, A., Godefroy, F., Gonzalez, Y.A., Guevara-Luna, M., Haque, S.M., Havenga, H., Herod, D., Hõrrak, U., Hussein, T., Ibarra, S., Jaimes, M., Kaasik, M., Khaiwal, R., Kim, J., Kousa, A., Kukkonen, J., Kulmala, M., Kuula, J., La Violette, N., Lanzani, G., Liu, X., MacDougall, S., Manseau, P.M., Marchegiani, G., McDonald, B., Mishra, S.V., Molina, L.T., Mooibroek, D., Mor, S., Moussiopoulos, N., Murena, F., Niemi, J.V., Noe, S., Nogueira, T., Norman, M., Pérez-Camaño, J.L., Petäjä, T., Piketh, S., Rathod, A., Reid, K., Retama, A., Rivera, O., Rojas, N.Y., Rojas-Quincho, J.P., San José, R., Sánchez, O., Seguel, R.J., Sillanpää, S., Su, Y., Tapper, N., Terrazas, A., Timonen, H., Toscano, D., Tsegas, G., Velders, G.J.M., Vlachokostas, C., von Schneidemesser, E., VPM, R., Yadav, R., Zalakeviciute, R., Zavala, M., 2021. A global observational analysis to understand changes in air quality during exceptionally low anthropogenic emission conditions. Environ. Int. 157, 106818 https://doi.org/10.1016/J.ENVINT.2021.106818.

Sulaymon, I.D., Zhang, Yuanxun, Hopke, P.K., Zhang, Yang, Hua, J., Mei, X., 2021. COVID-19 pandemic in Wuhan: ambient air quality and the relationships between criteria air pollutants and meteorological variables before, during, and after lockdown. Atmos. Res. 250, 105362 https://doi.org/10.1016/J.ATMOSRES.2020.105362.

Sun, Y., Lei, L., Zhou, W., Chen, C., He, Y., Sun, J., Li, Z., Xu, W., Wang, Q., Ji, D., Fu, P., Wang, Z., Worsnop, D.R., 2020. A chemical cocktail during the COVID-19 outbreak in Beijing, China: insights from six-year aerosol particle composition measurements during the Chinese New Year holiday. Sci. Total Environ. 742, 140739 https://doi.org/10.1016/J.SCITOTENV.2020.140739.

Targino, A.C., Gibson, M.D., Krecl, P., Rodrigues, M.V.C., dos Santos, M.M., de Paula Corrêa, M., 2016. Hotspots of black carbon and $PM_{2.5}$ in an urban area and relationships to traffic characteristics. Environ. Pollut. 218, 475–486. https://doi.org/10.1016/J.ENVPOL.2016.07.027.

USEPA, 2011. Exposure Factors Handbook Chapter 6-Inhalation Rates. U.S. Environmental Protection Agency.

Van den Bossche, J., Theunis, J., Elen, B., Peters, J., Botteldooren, D., De Baets, B., 2016. Opportunistic mobile air pollution monitoring: a case study with city wardens in Antwerp. Atmos. Environ. 141, 408–421. https://doi.org/10.1016/J.ATMOSENV.2016.06.063.

Venter, Z.S., Aunan, K., Chowdhury, S., Lelieveld, J., 2020. COVID-19 lockdowns cause global air pollution declines. Proc. Natl. Acad. Sci. USA 117, 18984. https://doi.org/10.1073/PNAS.2006853117, 18990.

Wallace, L.A., Wheeler, A.J., Kearney, J., Van Ryswyk, K., You, H., Kulka, R.H., Rasmussen, P.E., Xu, X., 2011. Validation of continuous particle monitors for personal, indoor, and outdoor exposures. J. Expo. Sci. Environ. Epidemiol. 21(1), 49–64. https://doi.org/10.1038/jes.2010.15.

Walsh, B.K., Hood, K., Merritt, G., 2011. Pediatric airway maintenance and clearance in the acute care setting: how to stay out of trouble. Respir. Care 56, 1424–1444. https://doi.org/10.4187/RESPCARE.01323.

Wang, D., Zhou, B., Fu, Q., Zhao, Q., Zhang, Q., Chen, J., Yang, X., Duan, Y., Li, J., 2016. Intense secondary aerosol formation due to strong atmospheric photochemical reactions in summer: observations at a rural site in eastern Yangtze River Delta of China. Sci. Total Environ. 571, 1454–1466. https://doi.org/10.1016/J.SCITOTENV.2016.06.212.

Wang, H., Miao, Q., Shen, L., Yang, Q., Wu, Y., Wei, H., 2021. Air pollutant variations in Suzhou during the 2019 novel coronavirus (COVID-19) lockdown of 2020: high time-resolution measurements of aerosol chemical compositions and source apportionment. Environ. Pollut. 271, 116298 https://doi.org/10.1016/J.ENVPOL.2020.116298.

WHO, 2020. WHO Director-General's opening remarks at the media briefing on COVID-19. 11 March 2020. accessed 11.11.21. https://www.who.int/director-general/speeches/detail/who-director-general-s-opening-remarks-at-the-media-briefing-on-covid-19-11-march-2020.